

# Impact ejecta characterization for small-sized fresh and degraded lunar craters using radar data

Ami J. Desai<sup>1,2</sup>, Shiv Mohan<sup>1</sup> and Sripada V. S. Murty<sup>1,\*</sup>

<sup>1</sup>PLANEX, Physical Research Laboratory, Ahmedabad 380 009, India

<sup>2</sup>Present address: Gujarat Institute of Disaster Management, Gandhinagar 382 009, India

**Ejecta distribution studies for large-sized (>10 km) lunar craters have been carried out earlier, but similar studies on smaller craters are lacking mainly due to data resolution limitations. Here we present a detailed quantification on spatial deposition of ejecta for small-sized lunar craters (<6 km). Using data from Mini RF instrument on-board NASA's Lunar Reconnaissance Orbiter, four Stokes parameters that differentiate and describe the observed backscattered electromagnetic field are calculated. We use the first Stokes parameter to investigate and estimate the spatial ejecta distribution for 98 small-sized fresh and degraded craters from mare and highland regions. It is observed that ejecta distribution can be described using power law with crater diameter and depth/diameter ( $d/D$ ) ratio. Ejecta behaviour is analysed for both the terrain types, highland and mare, enabling us to understand the effect and dependency of target rock properties on the ejecta characteristics. Further, the  $d/D$  dependence has indicated that the relative degradation rate appears higher for highland region compared to mare region.**

**Keywords:** Lunar impact craters, radar, spatial ejecta emplacement, target properties.

IMPACT cratering is the primary event in shaping a planetary surface through distribution and redistribution of ejecta material<sup>1-4</sup>. Craters serve as an important tool in deciphering valuable information on an evolutionary stages and surface properties of a planet<sup>5</sup>. Formation and emplacement of fresh ejecta is the foremost consequence of an impact event. The ejecta deposits are seen to be thickest and continuous near the crater rim and start thinning away as the distance increases from the rim. The portion of the ejecta deposit which is continuous and distinctly recognizable is termed as the ejecta blanket and is mostly observed to be extending ~1–2 crater radii from the crater rim for a crater of any diameter. For heavily cratered bodies in the Solar System, knowledge on the behaviour, amount and distribution of the ejecta generated is essential for the interpretation of local geology

and subsurface material, since the impact ejecta significantly modifies and influences the pre-existing surface in several remarkable ways<sup>4,6</sup>. The total ejecta emplacement extent, its absolute morphology and volume depend on various factors such as size, mass and velocity of the impactor, impact angle, target gravity, cohesiveness of the uppermost layer of the target rocks and atmospheric pressure of the planet. In case of the Moon, since it is completely devoid of atmospheric effects and has less surface gravity ( $1.622 \text{ ms}^{-2}$ ), the ejecta blanket is capable of extending several times the radius of the central crater.

Quantifying the ejecta matter in terms of mass and energy as a result of an impact<sup>7</sup> as well as estimating the amount of ejecta thickness and its total spatial distribution are still not well understood. Previously, using high-resolution miniature radio frequency (Mini-RF) polarimetric imaging radar studies on the estimation and assessment on how a discontinuous ejecta blanket lifetime varies with crater diameter had been attempted<sup>8</sup>. In view of similar dimensions, studies on crater analysis and characterization on the gradual change in the morphology of eroding ejecta blankets were also attempted using radar data<sup>9</sup>. The transitions between the radar bright and low backscatter within a given flow are now possible to be attributed to a range of surface roughness changes<sup>10</sup>, or due to the deposition of blocky material owing to topographic obstructions<sup>11</sup>, or changes in features similar to lava flows that form in impact melt<sup>12</sup>. However, the available data (both theoretical and geological) are not large enough for detailed estimates<sup>13</sup>. Our understanding on the knowledge on various lunar ejecta aspects has been greatly improved with the aid of recent high-resolution data which have effectively helped in discerning detailed information even from small diameter craters, which are of particular interest in view of the fact that they are (especially the ejecta) likely to be recent and better preserved than the larger ones<sup>6</sup>. The ejecta distribution and thickness studies for larger diameter craters using high-resolution optical and radar data have been attempted previously<sup>14</sup>. Using radar data, it has been shown that ejecta distribution depends upon the size of the craters<sup>15</sup>. The present study is extended for understanding the influence of various morphological parameters

\*For correspondence. (e-mail: murty@prl.res.in)

and target parameters on the model parameter. It has been carried out by creating a dataset for 98 small-sized craters (200 m to 6 km) using Mini RF and optical data covering parts of mare (32 fresh, 22 degraded craters) and highland (21 fresh, 23 degraded craters) regions. Details of these craters are provided in [Table S1; see Supplementary Information online](#).

## Rationale and approach

Impact ejecta studies are important for heavily cratered bodies like the Moon, where a systematic evaluation of the impact process, especially the amount, extent and distribution of the ejecta generated is largely essential for accurate interpretation and understanding of the local target rock geology and its effect over crater parameters such as depth, diameter and ejecta generated after an impact. Here we present a comprehensive observational analysis on the morphological characteristics of the small-sized craters (0.2–6 km), and the dependence of their spatial ejecta distribution on crater geometrical parameters. With regard to this, a detailed analysis on the ejecta distribution has been derived by direct measurements of crater ejecta using Mini-RF data covering mare and highland regions. Because of strong dependence of backscatter on surface roughness, radar images with high to medium backscatter can be classified as ejecta. Further, craters ranging within this diameter are mostly simple, bowl-shaped primary craters, produced as a result of meteoroid impact at speeds beyond a few kilometres/second. If the speed of the projectiles is lower (as in the case of secondary craters) it leads to irregular craters, which do not exhibit well-defined crater rims. It is also observed that unless the target strength is too high, simple craters can form randomly at any small diameter range, where the lower range is in inverse correlation with the gravity of the planet<sup>16</sup>. Large impact cratering can result in large-scale surface alterations<sup>6</sup>, at times giving rise to diverse flow features. Presently, for our measurements we make use of Mini-RF S band images having 12.6 cm wavelength and 30 m/pixel spatial resolution (zoom mode), which on this scale is highly sensitive to surface roughness, providing detailed information on the ejecta blanket with fine resolution and precision<sup>17</sup>. In addition, it also provides accurate ejecta estimation covering the entire proximal and distal parts within the same geological setting<sup>6</sup>, which otherwise was difficult to measure. Following an impact event, it is observed that the ejecta generated behaves differently depending on the target rock type. When an impactor with the same amount of kinetic energy strikes a surface, it is capable of producing ejecta on different spatial scales. Lunar surface is dominated by two major rock units: (1) mare region which is basaltic and highly rigid in nature, and (2) highland region composed of anorthosite and thus being frag-

ile in nature. As a result, impact energy is expected to dissipate to a much greater distance in highland region compared to mare region. Further, if an impact produces equal diameter craters in both the regions, the material excavated can be much higher for the highland region compared to mare region. The present study on the characterization of ejecta extent for fresh and degraded (mare and highland) lunar craters, aims to understand the dependence of ejecta extent on these parameters and on the physical attributes of the rock types.

## Study area

### *Lunar highland terrain craters*

For the present analysis, the highland craters correspond to the region in and around the NE-trending Rimae Sirsalis, believed to be a lunar graben and also the longest rille system on the Moon, covering a total distance of more than 400 km in length, less than 4 km wide (average), 150–230 m deep and located at 15.7°S 61.7°W. Located in the highlands south of Grimaldi, it is also the straightest rille on the lunar surface showing little branching and extensions<sup>18,19</sup>. As observed commonly, rilles are most often associated with mare, but the geological setting of Rimae Sirsalis is unique in a way that it almost entirely runs through the highland terrain.

### *Lunar mare terrain craters*

Fresh and degraded mare craters fall within five different mare terrains as mentioned below.

(1) Fresh and degraded lunar craters were analysed from Mare Crisium, which is located NE of mare Tranquillitatis. It is around 555 km in diameter, falling in the pre-Imbrium period. (2) The second region comprises craters in and around mare Serenitatis, located on the east of mare Imbrium. Falling within the Serenitatis basin of the Nectarian epoch, it is mostly composed of mare basalts. The coordinates are 28.0°N 17.5°E and it has a diameter of ~674 km. (3) Mare Imbrium having a diameter of 1146 km, is the second largest mare basin after Oceanus Procellarum. (4) Mare Fecunditatis, having a diameter of 840 km and formed during the pre-Nectarian epoch with material formed during the Upper Imbrium period exhibits an overlap with Nectaris, Tranquillitatis and Crisium basins. (5) Oceanus Procellarum, the largest mare basin covering 2500 km, is located on the western margin of the lunar near side. To its edges lie few other smaller mare regions, such as Mare Nubium and Mare Humorum.

In the present study, fresh and degraded craters from both the regions were analysed, although the sampling and mapping of fresh craters did present some limitations.

## Datasets

Lunar Reconnaissance Orbiter Camera (LROC)-derived wide angle camera (WAC) mosaic images; Mini-RF-derived S1 S band zoom mode images, and GLD 100 DTM data were used for the present study.

### *LROC WAC data for diameter measurements*

For the present study, LROC WAC mosaic images were used for measuring the crater diameter as well as for extracting information on the estimation of ejecta amount.

### *LRO Mini-RF data for ejecta extent measurements*

The Mini-RF system manifested on-board LRO is a light-weight synthetic aperture radar system (SAR) having two wavelengths operating in the X- and S-bands (4.2 and 12.6 cm respectively) with a spatial resolution of 30 m (zoom mode) and 150 m (baseline mode) respectively. The radar-returned information is characterized via classical Stokes parameters [S1, S2, S3, S4] which are then used for acquiring information on the radar scattering properties of the lunar surface<sup>4</sup>. Though for any detailed analysis surface composition and topography play a major role, the dominant factor affecting the total radar backscatter is roughness on the scale of the wavelength of the radar. Thus effectively a 12.6 cm Mini-RF total backscatter image measures the surface and near-subsurface roughness at scales of centimetres to decimetres, allowing prominent detection of the ejecta blankets deposited around the craters. In addition, since these images have a constant incidence angle of 48°, the sensitivity to ejecta blankets does not vary from image to image making Mini-RF an ideal tool for similar studies<sup>8,20–22</sup>.

### *GLD 100 data for depth measurements*

For obtaining precise information on the depth profile, GLD 100 data were used. The WAC digital terrain model (DTM) is constructed from WAC stereo images and the product obtained thereby is the global lunar DTM 100 m topographic model or GLD 100 model covering almost 98.2% of the lunar surface. About 44,000 LROC WAC stereo images have been tied with LOLA for computing GLD 100. It covers from 79°S lat. to 79°N lat.<sup>23–25</sup>. This combined product has a pixel spacing of 100 m with a vertical accuracy of 10–30 m. It is further observed that the mean difference between the heights of these two data is only about 4 m (ref. 26). Also, GLD 100 has lesser data gaps compared to Lunar Orbiter Laser Altimeter's (LOLA) limited cross-track coverage in the regions away from the poles<sup>27</sup>, facilitating a more comprehensive coverage.

## Methodology

Radar and WAC mosaic images having ample mappable samples of fresh and degraded craters (<6 km) from the mare and highland regions were downloaded from the Planetary Data System (PDS), integrated in ARC-GIS environment and geo-referenced. The selected fresh and degraded craters for both the regions were mapped and the total spatial ejecta distribution was calculated after a detailed demarcation for each individual crater as detailed earlier<sup>15</sup>. Our investigation included 98 craters.

### *Selection of fresh and degraded lunar craters*

Based on the distinct morphological characteristics, impact craters can be classified into fresh and degraded. Fresh craters usually exhibit bright albedo ejecta coverage<sup>28</sup>. With the passage of time, space weathering by micrometeorite bombardment together with galactic cosmic rays and high energy solar charged particles degrade the upper few centimetres resulting in lunar soil maturation. According to Bell *et al.*<sup>8</sup>, ejecta blankets of fresh lunar impact craters are expressed as halos of optical and radar bright material that gradually fade over the geological time period. Here we use radar-derived information to characterize the backscatter from a large number of ejecta blankets and classify them in two different categories: (1) fresh and (2) degraded. Fresh impact craters can be easily differentiated from older craters on the basis of their unique signatures obtained due to the presence of higher amount of blocky ejecta compared to degraded craters in which the estimates between rough and smooth material can be almost similar or exhibit less variation. Fresh craters usually display a sharp rim crest depending on the size of the crater. Fresh craters exhibiting rayed pattern fall into Copernican age and those without rays fall into Erathosthenian age, while slightly degraded to heavily degraded craters fall in Imbrium to pre-Imbrium age<sup>29</sup>. In general, fresh craters on terrestrial planets are surrounded by a continuous ejecta blanket extending to about 1–2 crater radii from the crater rim<sup>16,30</sup>. A characteristic feature which helps in detecting fresh craters is the presence of prominent rayed morphology. According to the observations from previous studies<sup>31</sup>, the maximum ray length attained by a ray crater is approximately in proportion to the size of the crater. The morphology of radar bright ejecta blankets of fresh impact craters is significantly shorter in the highlands than in mare region, possibly due to the effect of local topography and rock type. This also often creates difficulty in observing and analysing small-sized fresh craters from highland regions. Using remote-sensing imageries, lunar impact crater materials that are immature or recently disturbed or fresh are observed to be optically bright relative to their surroundings. Although, with time, due to the effect of space weathering,

prominent signatures helpful in identifying fresh ejecta may get subdued, the radar, owing to its longer wavelength can image such locations as well as further separate them into finer and coarser ejecta. This information can be expressed using derived products such as the circular polarization ratio (CPR). Mini-RF is specifically designed to differentiate various crater properties<sup>32</sup>.

Nonetheless, studies on small-sized craters always offer certain discrepancies. Sufficient samples for fresh craters fulfilling all the required criteria for proper analysis were at times difficult to be traced out. On the other hand, in the case of degraded craters, they often tend to exhibit varying levels of crater degradation; from relatively fresh ones to partially decayed, completely decayed or showing different levels of material slumping and infilling in response to subsequent impacts. Nevertheless, in order to avoid large discrepancies arising out of such processes, care was taken while selecting the crater. Only those craters, although necessarily degraded ones, falling into a measurable range were opted. Figure 1 shows an example of fresh and degraded crater morphology and also how on the basis of surface roughness two types of ejecta can be distinctly classified and differentiated.

#### *Depth and diameter measurements*

Diameter of each crater was obtained from WAC data by taking rim-to-rim dimensions. Similarly, average depths were also estimated using GLD 100 profiles. Since the amount of ejecta excavated after an impact also depends on the excavated crater depth, a variation in the depth diameter to the amount of ejecta excavated is observed<sup>33</sup>.

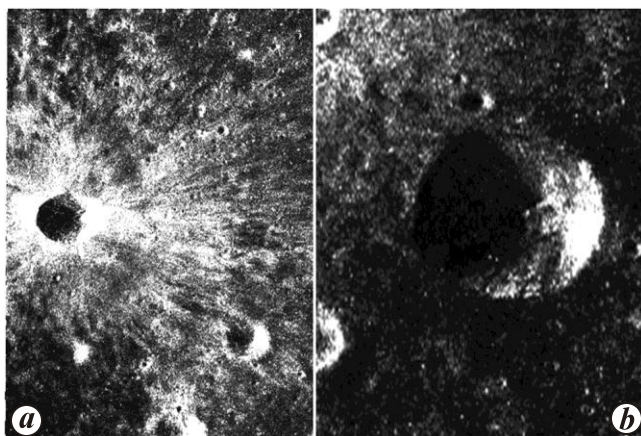


**Figure 1.** Illustrative diagram showing Mini RF image of (a) fresh and (b) degraded craters. The brighter regions are those showing high backscatter categorized into more rough or inner continuous blocky ejecta, whereas the regions with lower brightness depict outer discontinuous finer ejecta matter (crater diameter 0.51 km and 5 km, coordinates  $-18.13, -64.77$  and  $-18.97, -65.84$  respectively).

#### *Ejecta extent measurements*

Mini-RF on-board LRO utilizes new wideband hybrid polarization architecture to measure Stokes parameters of the reflected signal<sup>22</sup>. In the present study, in order to obtain the estimates on the spatial ejecta extent, we make use of Stokes parameter 1 ( $S_1$ ), which is the sum of the horizontal and vertical linear polarization channels providing the intensity information. Here the pixel brightness displays the intensity of the backscattered return<sup>9</sup>. The excavated material which is deposited in the form of ejecta blanket after an impact event principally depends on the excavation depth, local topography, rock type and slope effects. Based on these parameters and the viscosity of the ejecta, it settles and gets distributed around a crater. Because of SAR sensitivity for ejecta and its roughness, it is possible to derive a close estimate of the spatial ejecta extent<sup>34</sup>. Several factors play a role in contributing towards variable backscatter intensity. The first and most important parameter is the topographical slope along the look direction. Higher signal is expected to be reflected back if the slope angle is towards the spacecraft, whereas lower signal is reflected back if the slope is angled away from the spacecraft. As a consequence, brightened wall will be angled towards the spacecraft, whereas the darkened wall is angled away from the spacecraft. Another important factor determining the backscatter intensity is the surface roughness on the scale of the wavelength of the radar. For instance, the S-band on the Mini-RF has a wavelength of 12.6 cm; so it scatters back to the receiver most strongly when the surface it is observing has a large number of decimetre-sized blocks<sup>17</sup>. The transition from bright to low backscatter reflects the boundary of more blocky to smoother ejecta with reference to the radar wavelength. Finer material corresponds to an increasing fraction of the total ejecta volume with increasing distance from the crater. Therefore, ejecta are generally darker as distance increases from the crater<sup>35</sup>. Thus based on the radar response for surface roughness, the ejecta have been categorized into two tonal variations. Higher backscatter displays a prominent bright tone, whereas the lower backscatter displays a comparatively darker tone. The dark ejecta have a backscatter coefficient value of about  $-10$  dB, whereas the bright ejecta are represented by a value of  $-2.0$  dB corresponding to greater roughness. Considering this fact, in order to derive accurate information on the spatial ejecta extent, we mapped, classified and categorized the ejecta into two groups. (1) Coarse ejecta where the amount of deposition is more hummocky/blocky and exhibits a prominent brighter tone as a result of high backscattering. Further, this material is expected to be deposited largely in close vicinity of the impact due to its larger and heavier particle size. (2) Finer ejecta where the amount of ejecta deposition near the impact point is lesser than in case of coarse ejecta, but the total area covered is larger because of smaller particle

size. It also exhibits a prominent low backscatter. The total ejecta deposit extent is estimated by combining both these types of deposition. Various statistical regressions were than studied and analysed.

Selection of any particular parameter, viz. crater rim for diameter, depth, or the ejecta extent needs extremely precise pixel demarcation, especially at the edges, which may not be accurately possible leading to pixel measurement errors. This type of measurement errors occurs especially when the crater boundary is not well-defined or/and if there is marked low image contrast which makes a precise delineation difficult. To minimize errors due to this, care has been taken while selecting the craters, and later on by taking repeated and multiple measurements for each of the required parameters.

### Data analysis

Ejecta is deposited either in a continuous or discontinuous fashion termed as ejecta blanket. Continuous ejecta blankets are typically blocky and exhibit high albedo when fresh<sup>16</sup>. The maximum boulder diameter in an ejecta blanket increases with increase in the crater size<sup>30,36</sup>. A variable intensity is thus observed in the radar images, which essentially depends on the ejecta block size. In most of the cases, a clear dichotomy is observed between the continuous and discontinuous ejecta. The coarser ejecta consisting of larger blocks is mostly seen to be occupying the inner locations settling at a shorter distance compared to finer material which is deposited nearer as well as at a much farther distances from the crater rim (Figure 1). Often, they are observed to exhibit spectacular long arrays of radiating ejecta, also termed as rayed pattern, which is one of the most common morphological parameters considered for detecting fresh craters<sup>37</sup>. Depending on the difference in the target rock strength, we observed depth variability for similar to nearly similar-sized craters. The mare region is comprised of basalts, and owing to its compact and hard-rock nature is expected to show less ejecta excavation. In contrast, the highland region is comprised of anorthosites and would spill more ejecta owing to its fragile nature. The more cohesive nature of basalts can be attributed to its higher density ( $\sim 2.8$  to  $3.2 \text{ g/cm}^3$ )<sup>38</sup> and cohesive strength compared to anorthosites having lower density ( $\sim 2.5$ – $2.8 \text{ g/cm}^3$ )<sup>38</sup>. For our measurements and analysis, fresh craters which met the following two important criteria were considered: (1) diameter  $\geq 0.2 \text{ km}$  and (2) radar-bright halo diameter  $\geq 6$  crater diameters, i.e. about 12 crater radii of continuous ejecta blanket beyond the crater rim<sup>8</sup>.

### Characterization of craters based on $d/D$ ratio

Relationship between depth/diameter ( $d/D$ ) till now has been mostly analysed for larger diameter craters, but

considering the importance of understanding the morphologies of small-sized craters, the present study has been undertaken. In general, ratio of  $d$  to  $D$  has been used for characterizing the shape of craters using a simple power law  $d = c_1 D^{c_2}$ , where  $c_1$  and  $c_2$  are constants<sup>16</sup>. Typical  $d/D$  has long been known to be  $\sim 0.2$  for primary simple craters on the Moon<sup>39</sup>. In the present study, we observed steeper slope (0.033) compared to Daubar *et al.*<sup>40</sup> for small craters, and Pike<sup>39</sup> for large craters (Figure 2). A deviation from 0.2 may result due to crater degradation, measurement errors arising due to small size of craters and target properties as indicated by Daubar *et al.*<sup>40</sup> for small-sized craters. Our observations also present similar deviation from 0.2 as indicated by Daubar *et al.*<sup>40</sup> for the 0.2–6 km size craters. Effect of target properties and crater degradation play a role in lowering the expected  $d/D$ , especially for this range of crater diameter. For small-sized craters, ejecta slumping and erosion with time would be at faster rate resulting in faster infilling of the crater, thereby decreasing the crater depth.

### Relation of crater diameter and spatial ejecta extent

The ejecta extent is expected to increase with an increase in the crater diameter<sup>15</sup>. However, the rheological properties of the target material also play a role in this regard. In order to understand variability of ejecta extent, we carried out a systematic analysis on the relation between

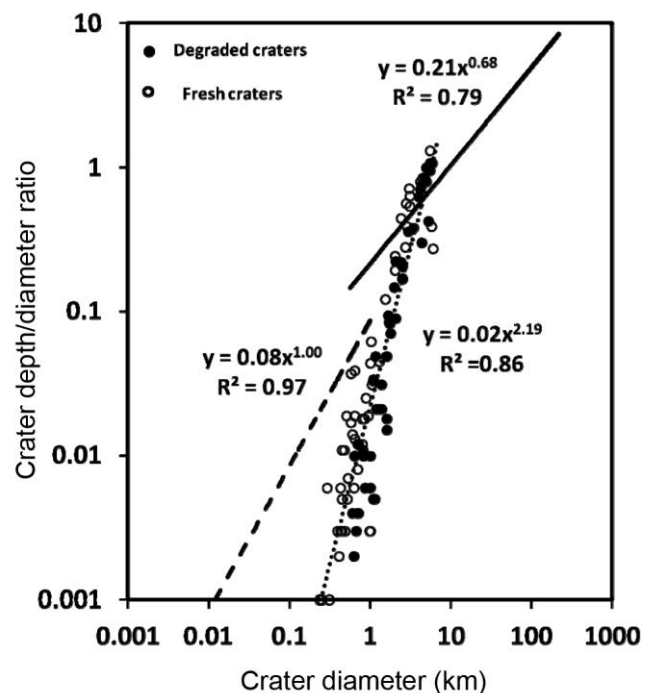


**Figure 2.** Combined fit showing diameter (km) versus depth/diameter ratio for craters below 1 km (---, Daubar *et al.*<sup>40</sup>), 0.2 to 6 km (....., the present study) and beyond 1 km (—, Pike<sup>39</sup>).

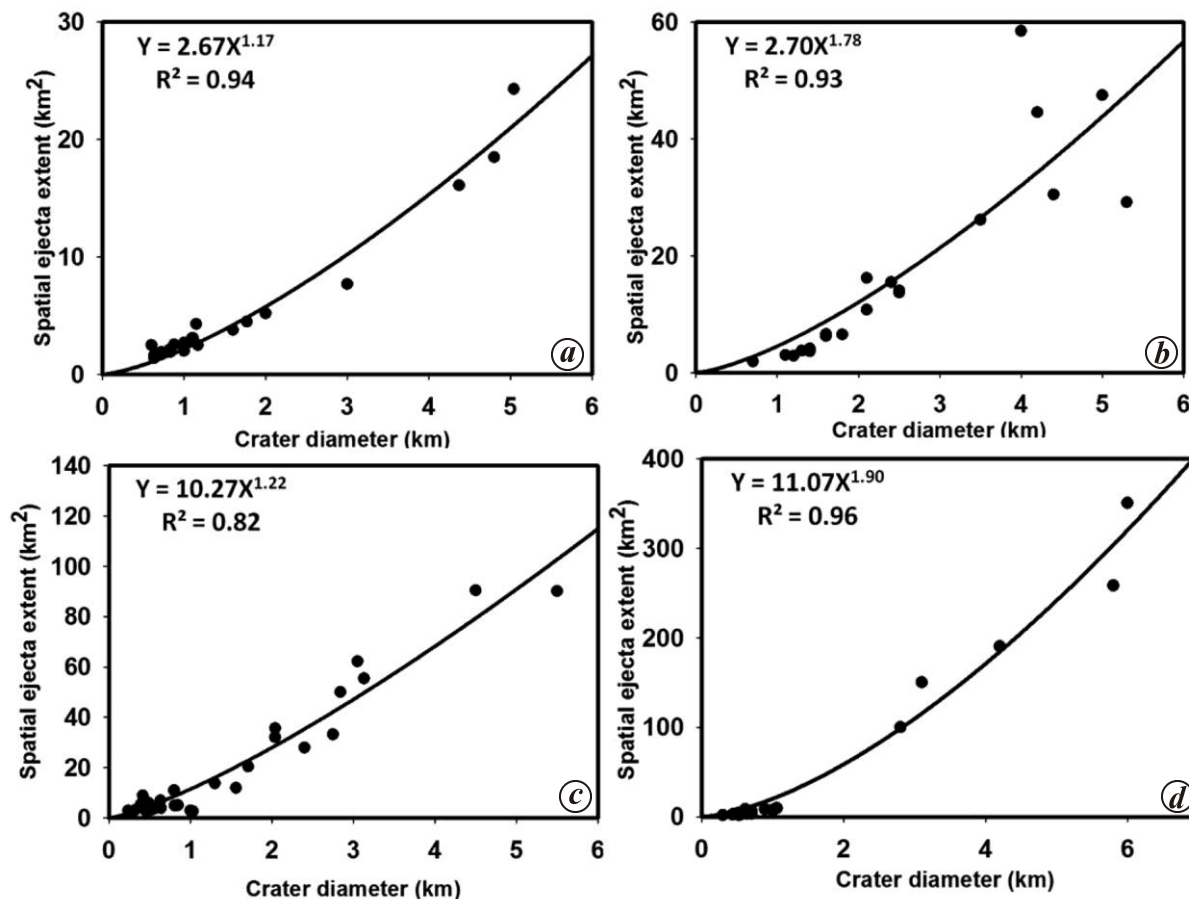


Figure 3a–d. Relation between crater diameter and spatial ejecta extent within (a) mare degraded, (b) highland degraded, (c) mare fresh and (d) highland fresh regions.

crater diameter and the ejecta extent. The results are categorized into four groups, namely highland craters (fresh and degraded) and mare craters (fresh and degraded). For each category, the diameter of the crater was plotted against the total ejecta extent and the relationship was examined for exponential, power and polynomial fitting. It was observed that the data fit best by power law relation (eqs (1)–(4)), for all the categories as given below

- For highland degraded craters  $Y = 2.70X^{1.78}$ , (1)
- for highland fresh craters  $Y = 11.1X^{1.9}$ , (2)
- for mare degraded craters  $Y = 2.67X^{1.17}$ , (3)
- for mare fresh craters  $Y = 10.27X^{1.22}$ , (4)

where  $X$  and  $Y$  are crater diameter and ejecta extent respectively.

The principal observations from these models are as follows:

(1) Figure 3a and b shows the variation of spatial ejecta extent with crater diameter for mare and highland

degraded craters. Data for both the regions show a positive correlation demonstrating a consistent increase of spatial ejecta extent with an increase in the crater diameter, which could be described by the power law. The power law equations of mare degraded and highland degraded craters (considering similar types of craters but varying terrains) give different exponent values of 1.17 and 1.78 with  $R^2 = 0.94$  and  $R^2 = 0.93$  respectively, though the constants for the highland region (2.7) and mare region (2.67) are similar. The model error of estimation is expected to be ~8.4% and 1.2% for highland and mare degraded craters respectively.

The higher value of the exponent for highland degraded craters implies and supports the fact that for an almost equivalent impact, the highland terrain is capable of excavating greater amount of ejecta material due to its lower cohesive strength and fragile nature compared to mare basalt. This results in larger spatial ejecta coverage over a surface.

(2) The power law equations for mare fresh and highland fresh craters (considering similar types of craters but varying terrains) also give different values of 1.22 and 1.9 with  $R^2 = 0.82$  and  $R^2 = 0.96$  respectively, for the

exponent (Figure 3 *c* and *d*), similar to the case of degraded craters. The values of these exponents are similar to their corresponding counterparts in degraded craters. But the values of the constants for the fresh craters in case of both highland and mare regions are higher at 11.07 and 10.27 respectively, compared to the case of degraded craters. This clearly shows that in addition to the target rock rheology, the ejecta extent depends on the freshness of the crater. Obviously, degradation decreases the ejecta extent. The model error of estimation is 6.1% and 16% respectively, for mare and highland fresh craters.

(3) A comparison between mare degraded and mare fresh craters shows that though the values of exponents 1.17 ( $R^2 = 0.94$ ) and 1.22 ( $R^2 = 0.82$ ) are almost similar (Figure 3 *a* and *c*), value of constant is much higher for mare region fresh craters (10.27) compared to mare region degraded craters (2.7). This explains that the spatial ejecta extent in mare fresh craters is larger than the degraded craters due to decay of ejecta extent over a period of time. The model error of estimation is 6.1% and 1.2% respectively, for mare fresh and mare degraded craters.

(4) Similarly, for highland degraded and highland fresh craters (considering varying types of craters but similar terrains), the power law relation gives similar value of 1.78 ( $R^2 = 0.93$ ) and 1.9 ( $R^2 = 0.96$ ) respectively, for the exponent (Figure 3 *b* and *d*) and different values of constant, being much higher for fresh craters case (11.07) than that for degraded craters (2.7). The model error of estimation is 16% and 8.4% respectively.

The values suggest that the spatial ejecta extent distribution in fresh craters is much higher than that of degraded craters and also indicates the degradation of ejecta with time. The degraded craters would have undergone weathering with time, resulting in the reduction of the total preserved material. Similar conclusion holds good for mare fresh versus mare degraded craters, given in case (3).

Overall, our analysis shows a positive correlation between the crater diameter and total ejecta extent, whereby the ejecta extent gradually and consistently increases with increase in crater diameter. This implies that the amount of material excavated after an impact event strongly and largely depends on the crater diameter. The study also indicates a strong dependence of surface material on the amount of ejecta excavated. Moreover, it can be observed that the highland region which is anorthositic tends to excavate larger amount of ejecta than the mare region composed of basalt, for similar crater diameter, owing to the variation in the original depth attained after an impact depending on the terrain lithological properties<sup>5</sup>. Further, considering the fact that the fresh craters in mare and highland should have greater preserved ejecta compared to the degraded ones, the highland region fresh craters are observed to excavate highest amount of ejecta. This again demonstrates the effect of surface material on ejecta distribution. It is observed that the exponent values for fresh craters in both the regions are higher, which also explains

that for fresh craters the amount of ejecta retained and preserved is much higher than in case of degraded craters. Moreover, considering any inter-correlation, it has always been observed that the highland region in all the cases shows higher amount of ejecta compared to mare basalt. Thus our study demonstrates that the target rock strength factor plays a vital role in the spatial distribution of ejecta over a planetary surface.

In the power law relations ( $Y = AX^B$ ), the values of constant  $A$  and exponent  $B$  clearly indicate a trend. For highland craters, the value of  $B$  is similar for both fresh and degraded craters, while the value of  $A$  is much higher for fresh craters. For mare craters as well  $B$  is similar between fresh and degraded craters, while  $A$  is high for fresh craters. Though the values of constant and the trend between highland and mare craters are parallel, the values of exponents are different and relatively higher for the highland craters. We can infer that the value of  $B$  is dependent on target properties (density and cohesive strength), while the value of  $A$  is a measure of degradation.

#### *Relation of $d/D$ ratio and spatial ejecta extent*

Information on the changes in the  $d/D$  ratio over a planetary surface gives knowledge on the transition regions such as the change in the crater type; from simple to complex, or on the region where there may be a change based on gravity or surface strength<sup>5</sup>. Further, variations in  $d/D$  can also reflect on the target material strength, impact velocity and impact angle, which play an important role in establishing the crater depth<sup>40</sup>. Earlier studies have suggested that the  $d/D$  ratio decreases with the passage of time due to continuous crater degradation and material infilling<sup>41</sup>. At the same time, the spatial ejecta would fade and degrade leading to a slow but continuous decrease in the spatial ejecta extent. Thus,  $d/D$  could also have a relationship with ejecta extent. In view of this, we have examined the relationship between ejecta extent and  $d/D$  for the fresh and degraded craters covering mare and highland regions using data from 98 craters. Following are the empirical relations describing the  $d/D$  ratio with crater ejecta extent

$$\text{For highland degraded craters } Y = 191.5X^{0.88}, \quad (5)$$

$$\text{for highland fresh craters } Y = 460.4X^{1.08}, \quad (6)$$

$$\text{for mare degraded craters } Y = 33.3X^{0.57}, \quad (7)$$

$$\text{for mare fresh craters } Y = 119.44X^{0.69}, \quad (8)$$

where  $X = d/D$  and  $Y$  is crater ejecta extent.

Following are details of the analysis:

(1) Correlation between  $d/D$  ratio and total ejecta distribution for mare degraded and highland degraded

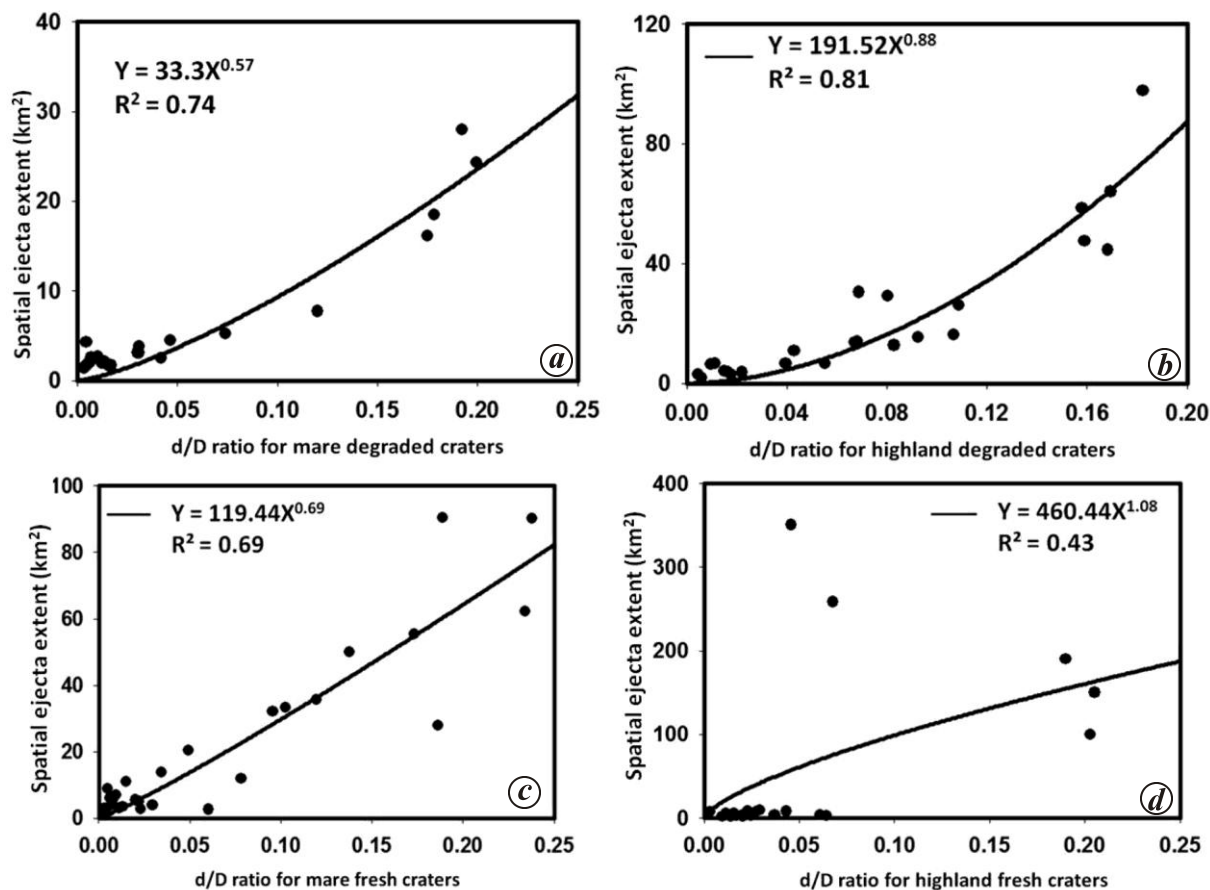


Figure 4 a–d. Relation between depth/diameter ( $d/D$ ) ratio and total ejecta excavated within (a) mare degraded, (b) highland degraded, (c) mare fresh and (d) highland fresh regions.

craters gives exponent values of 0.57 and 0.88 with  $R^2$  value as 0.74 and 0.81 respectively (Figure 4 a and b). Regarding the total extent of ejecta coverage, it is evident from the data and values that initially the amount of ejecta attained in case of highland appears to be much higher than that in case of mare craters. The constant value in case of highland region is significantly higher (191.5) than that in mare region (33.3). This also supports the fact that an impact in highland rock initially would have excavated more ejecta material compared to the mare region.

In addition, from a comparative analysis of the data plots as well as from the model fit values of ejecta distributed on the basis of diameter and  $d/D$ , it is evident that in all the cases the ejecta amount appears to be higher for highland region compared to mare. Moreover, using  $d/D$  as a parameter, the model provides better explanation on the effect of target properties for the ejecta distribution in the case of fresh and degraded craters. It is observed that the value of the constant is higher in case of highland than the mare for degraded craters. Further, the value of the exponent is higher for highland compared to mare, which is indicative of rate of degradation. Therefore, degradation is faster in highland compared to mare.

Such observations have also been reported by Fassett and Combellick<sup>42</sup>. The present analysis thus strongly emphasizes the role of target on ejecta distribution and its further degradation.

(2) Correlation between  $d/D$  ratio of mare fresh and highland fresh craters gives power values of 0.69 and 1.08 with  $R^2 = 0.69$  and  $R^2 = 0.43$  respectively (Figure 4 c and d). The constant value in the power law equation for highland region (460.4) is greater than in case of mare region (119.4). These results, although for fresh craters, also correspond in a similar fashion, as detailed in case (1). The higher values of exponent and constant for fresh craters from highland region correspond to a higher degree of ejecta excavation and distribution with respect to depth and diameter. Again it shows that degradation is faster in highland compared to mare<sup>42</sup>.

The value of  $R^2$  especially for the highland fresh craters is poor. This is due to the relatively smaller number of available samples for highland fresh craters within our defined study region. Also, small craters ( $d/D < 0.05$ ) do not show significant ejecta distribution, thus influencing the model correlation coefficient. However in spite of the limitations, the existing data do show the expected trend and results. In addition to considering all these probable

factors, we also believe that the results can be improved and show a better trend if we do not restrict our study region for obtaining highland fresh crater samples.

Through this study we observe a strong and consistent relation between  $d/D$  with total ejecta based on varying terrain types. Relation between  $d/D$  and total ejecta excavated appears to be a strong indicator for examining crater degradation with time for small-sized lunar craters. Further, the results are also consistent based on the ejecta derived from the varying types of craters (fresh and degraded). The empirical relations are described by the power law and model coefficients are observed to be strongly governed by target properties and crater degradation. Differences represented by the power law relations for fresh and degraded craters for mare and highland regions suggest that the exponent in the fit equations reflects the target characteristics, while the value of the constant reflects the extent of degradation.

## Conclusion

Observations from radar data show distinct signature of crater ejecta due to its sensitivity to surface roughness. Thus, it is possible to estimate the ejecta extent using variable radar backscatter measurements. On analysing various datasets and their interdependence on crater geometrical parameters such as crater depth and diameter, and also taking into consideration the changes caused in response to varying target rock types and strength, we conclude that the total spatial ejecta extent can be directly correlated with crater diameter and crater depth/diameter ( $d/D$ ) ratio. An assessment on the relationship of  $d/D$  ratio and spatial ejecta extent and its variation in response to target properties shows similar results for fresh and degraded craters in highland and mare regions. The present study demonstrates a new method for studying the relationship of ejecta extent with crater geometry and degradation state. Based on our analysis for 98 craters, it can be concluded that for small-sized craters, the spatial ejecta distribution can be described by the power relation with crater diameter as well as with crater depth/diameter ratio.

1. Werner, S. C. and Medvedev, S., The lunar rayed-crater population – characteristics of the spatial distribution and ray retention. *Earth Planet. Sci. Lett.*, 2010, **295**, 147–158.
2. Patterson, G. W., Cahill, J. T. S. and Bussey, D. B. J., Characterization of lunar crater ejecta deposits using radar data from the Mini-RF instrument on LRO. In 44th Lunar and Planetary Science Conference, Abstr. #2380, USA, Houston, Texas, 18–22 March 2013.
3. Stickle, A. M., Patterson, G. W., Bussey, D. B. J., Cahill, J. T. S., and Mini-RF team, Mini-RF observations of mare ejecta emplacement diversity. In Annual Meeting of the Lunar Exploration Analysis Group, Abstr. #3064, Laurel, Maryland, USA, 22–24 October 2014.
4. Patterson, G. W., Stickle, A. M., Bussey, D. B. J., Cahill, J. T. S. and Mini-RF team, Mini-RF observations of the radar scattering properties of young lunar crater ejecta blankets. In 45th Lunar and Planetary Science Conference, Abstr. #2720, USA, Houston, Texas, 17–21 March 2014.
5. Vincent, J. B. *et al.*, Crater depth-to-diameter distribution and surface properties of (4) Vesta. *Planet. Space Sci.*, 2014, **103**, 57–65.
6. Wells, K. S. and Bell III, J. F., Characterization of ejecta facies of a small lunar crater in Balmer Basin using LROC data. In 41st Lunar and Planetary Science Conference, Abstr. #1932, USA, Houston, Texas, 1–5 March 2010.
7. O’Keefe, J. D. and Ahrens, T. J., Impact ejecta on Moon. In Proceedings of the 7th Lunar Science Conference, USA, Houston, Texas, 15–19 March 1976, pp. 3007–3025.
8. Bell, S.W., Thomson, B. J., Dyar, M. D., Neish, C. D., Cahill, J. T. S. and Bussey, D. B. J., Dating small fresh lunar craters with mini-RF radar observations of ejecta blankets. *J. Geophys. Res.*, 2012, **117**, E00H30; doi:10.1029/2011JE004007.
9. Bell, S. W., Fresh lunar crater ejecta as revealed by the miniature radio frequency (Mini-RF) instrument on the Lunar Reconnaissance Orbiter. Thesis submitted for degree of Bachelor of Arts with Honors, Department of Astronomy, Amherst College, United States, 2011.
10. Chadwick, D. J. and Schaber, G. G., Impact crater outflows on Venus: morphology and emplacement mechanisms. *J. Geophys. Res. (Planets)*, 1993, **98**(E-11), 20891–20902.
11. Schultz, P. H., Atmospheric effects on ejecta emplacement and crater formation on Venus from Magellan. *J. Geophys. Res.*, 1992, **97**(E10), 16183–16248.
12. Johnson, J. R. and Baker, V. R., Surface property variations in Venusian fluidized ejecta blanket craters. *Icarus*, 1994, **110**, 33–70.
13. French, B. M., *Traces of Catastrophe, A Handbook of Shock – Metamorphic Effects in Terrestrial Meteorite Impact Structures, Impact Melts*, LPI Contribution No. 954, Lunar and Planetary Institute, 1998, vol. 120, pp. 79–90.
14. Morota, T. *et al.*, Ejecta thickness of lunar impact basin. In 42nd Lunar and Planetary Science Conference, Abstr. #1301, USA, Houston, Texas, 7–11 March 2011.
15. Desai, A. J., Shiv Mohan and Murty, S. V. S., Lunar crater ejecta distribution and characterization using Mini-RF and LROC-WAC data. *Curr. Sci.*, 2014, **107**, 824–831.
16. Melosh, H. J., *Impact Cratering: A Geologic Process*, Oxford University Press, New York, 1989, p. 245.
17. Neish, C. D., Bussey, D. B. J., Spudis, P., Marshall, W., Thompson, B. J., Patterson, G. W. and Carter, L. M., The nature of lunar volatiles as revealed by Mini-RF observations of the LCROSS impact site. *J. Geophys. Res.*, 2011, **116**, E01005; doi: 10.1029/2010JE003647.
18. North, G., *Observing the Moon, The Modern Astronomer’s Guide*, Cambridge University Press, 2000, pp. 324–328; p. 381.
19. Head, J. W., Wilson, L., Anderson, K. A. and Lin, R. P., Tectonic processes on planets and satellites, lunar linear rilles, models of dike emplacement and associated magnetization features. In Lunar and Planetary Science Conference 28, USA, Houston, Texas, 17–21 March 1997, pp. 541–542.
20. Raney, K. R., Hybrid-polarity SAR architecture. *IEEE Trans. Geosci. Remote Sensing*, 2007, **45**, 3397–3404; doi:10.1109/TGRS.2007.895883.
21. Bussey, D. B. J., Spudis, P. D., Nozette, S., Lichtenberg, C. L., Raney, R. K., Marinelli, W. and Winters, H. L., Mini-RF: imaging radars for exploring the lunar poles. In 39th Lunar and Planetary Science Conference, Abstr. #2389, USA, Houston, Texas, 10–14 March 2008.
22. Nozette, S. *et al.*, The Lunar Reconnaissance Orbiter miniature radio frequency (Mini-RF) technology demonstration. *Space Sci. Rev.*, 2010, **150**, 285–302; doi:10.1007/s11214-009-9607-5.
23. Scholten, F., Oberst, J., Matz, K. D., Roatsch, T., Wählisch, M., Robinson, M. S. and LROC Team, GLD 100 – the global lunar

## RESEARCH ARTICLES

---

- 100 meter raster DTM from LROC WAC stereo models. In 42nd Lunar and Planetary Science Conference, Abstr. #2046, Texas, 7–11 March 2011.
24. Scholten, F., Oberst, J. and Robinson, M. S., GLD100 – lunar topography from LROC WAC stereo. In EPSC Abstr., EPSC-DPS2011-1272-1, 2011, vol. 6.
25. Scholten, F., Oberst, J., Matz, K. D., Roatsch, T., Wählisch, M., Speyerer, E. J. and Robinson, M. S., GLD100 – the near-global lunar 100 meter raster DTM from LROC WAC stereo image data. *J. Geophys. Res.*, doi:10.1029/2011JE003926.
26. Scholten, F. *et al.*, Complementary Global LRO lunar topography datasets – a comparison of 100 m raster DTMs from LROC WAC Stereo (GLD 100) and LOLA altimetry data. In 42nd Lunar and Planetary Science Conference, Abstr. #2080, USA, Houston, Texas, 7–11 March 2011.
27. Bray, V. J., Stone, C. A. and McEwen, E. A., Investigating the transition from central peak to peak-ring basins using central feature volume measurements from the global lunar DTM 100 m. *Geophys. Res. Lett.*, 2012, **39**, L21201; doi: 10.1029/2012GL053693.
28. Craddock, R. A. and Howard, A. D., Simulated degradation of lunar impact craters and a new method for age dating farside mare deposits. *J. Geophys. Res.*, 2000, **105**(E-8), 20387–20401.
29. Cintala, M. J., Head, J. W. and Mutch, T. A., Characteristics of fresh Martian craters as a function of diameter: comparison with the Moon and Mercury. *Geophys. Res. Lett.*, 1976, **3**(3), 117–120; doi:10.1029/GL003i003p00117.
30. Osinski, G. R., Tornabene, L. L. and Grieve, R. A. F., Impact ejecta emplacement on terrestrial planets. *Earth Planet. Sci. Lett.*, 2011, **310**, 167–181.
31. Baldwin, R. B., *The Measure of the Moon*, University of Chicago Press, USA, 1963, p. 508.
32. Patterson, G. W., Raney, R. K., Cahill, J. T. S., Bussey, D. B. J. and the Mini-RF team, Characterization of lunar crater ejecta deposits Using m–chi decompositions of Mini-RF radar data. In EPSC Abstr., EPSC2012-731, European Planetary Science Congress, 2012, vol. 7.
33. Pike, R. J., Depth/diameter relations of fresh lunar craters: revision from spacecraft data. *Geophys. Res. Lett.*, 1974, **1**(7), 291–294; doi:10.1029/GL001i007p00291.
34. Cahill, J., Patterson, G. W., Raney, R. K., Bussey, B., Turtle, E. P. and Mini RF science team, Mini-RF’s perspective of the lunar Western hemisphere and Orientale basin’s ejecta deposits. American Geophysical Union, Fall Meeting, Abstr. #P13G-08, 2011.
35. Ghent, R. R., Campbell, B. A., Hawke, B. R. and Campbell, D. B., Earth-based radar data reveal extended deposits of the Moon’s Orientale basin. *Geology*, 2008, **36**, 343–346; doi:10.1130/G24325A.1.
36. Bart, G. D. and Melosh, H. J., Using lunar boulders to distinguish primary from distant secondary impact craters. *Geophys. Res. Lett.*, 2007, **34**, doi:10.1029/2007GL029306.
37. Schultz, P. and Lutz-Garihan, A., Grazing impacts on mars: a record of lost satellites. *J. Geophys. Res.*, 1972, **87**, A84–A96.
38. Martel, L. M. V., Lunar rock densities – PSRD a CosmoSparks report. 2012; <http://www.psrdr.hawaii.edu/CosmoSparks/July12/Lunar-rock-densities.html>
39. Pike, R. J., Apparent depth/apparent diameter relation for lunar craters. In Proceedings of the 8th Lunar Science Conference, USA, Houston, Texas, 14–18 March 1977, pp. 3427–3436.
40. Daubar, I. J., Stone, C. A., Byrne, S., McEwen, A. S. and Russell, P. S., The morphology of fresh craters on Mars and Moon. *J. Geophys. Res. (Planets)*, 2014, **119**(E-12), 2620–2639, doi: 10.1002/2014JE004671.
41. Stopar, J. D., Robinson, M. S., Speyerer, E. J., Burns, K., Gengl, H. and LROC team, Regolith characterization using LROC NAC digital elevation models of small lunar craters. In 43rd Lunar and Planetary Science Conference, Abstr. #2729, USA, Houston, Texas, 19–23 March 2012.
42. Fassett, C. I. and Combellick, J. R., The rate of crater degradation and topographic evolution on the Moon: results from the Maria and Initial comparisons with the highlands. In 45th Lunar and Planetary Science Conference, Abstr. #1429, USA, Houston, Texas, 17–21 March 2014.

ACKNOWLEDGEMENTS. We thank the anonymous reviewer for his valuable suggestions. We also thank the Department of Space, Government of India for financial support to carry out this work.

Received 8 July 2015; revised accepted 25 November 2015

doi: 10.18520/cs/v110/i10/1929-1938

---